Available online at www.sciencedirect.com
ScienceDirect
Journal of Solid State Chemistry 181 (2008) 2006–2019
JOURNAL OF SOLID STATE CHEMISTRY
www.elsevier.com/locate/jssc

Characterization and reactivity of nanoscale La(Co,Cu)O_3 perovskite catalyst precursors for CO hydrogenation

Nguyen Tien-Thao[a], Houshang Alamdari[b], Serge Kaliaguine[a,*]

[a]*Department of Chemical Engineering, Laval University, Quebec, Canada G1K 7P4*
[b]*Department of Mining and Metallurgy, Laval University, Quebec, Canada G1K 7P4*

Received 12 June 2007; received in revised form 30 October 2007; accepted 10 November 2007
Available online 22 November 2007

Abstract

The characterization of La(Co,Cu)O_3 perovskites has been performed by several techniques including XRD, BET, H_2-TPR, O_2-TPO, TPRS, and the solids tested as catalysts for the hydrogenation of CO. The reducibility of the perovskites is strongly affected by the preparation route, calcination temperature, catalyst morphology, and the amount of remnant alkali. Compared with the citrate-derived perovskite, $LaCoO_3$ sample prepared by mechano-synthesis has various distinct Co^{3+} ions in perovskite lattice, which are reduced at different temperatures. Under typical conditions, the reduction of cobalt ions occurs in two consecutive steps: Co^{3+}/Co^{2+} and Co^{2+}/Co^0, while the intra-lattice copper ions are directly reduced from Cu^{2+} to Cu^0. The reducibility of cobalt ions is promoted by the presence of metallic copper, which is formed at a lower reduction temperature. The re-oxidation of the reduced lanthanum cobaltite perovskite could regenerate the original structure, whereas that of the reduced Co–Cu-based samples is less reversible under the same experimental conditions.

The cobalt atom in the reduced perovskites plays an important role in the dissociation of CO, but the presence of a neighboring copper along with remnant sodium ions on the catalyst surface has remarkably affected the reactivity of cobalt for CO hydrogenation. The addition of copper into the perovskite framework leads to a change in the product distribution of CO hydrogenation and a decrease in reaction temperature. An increased copper content leads to a substantial decline in the rate of methanation and an increase in the formation of higher alcohols. A close proximity between cobalt and copper sites on the Na^+-modified catalyst surface of the reduced nanocrystalline Co–Cu-based perovskites plays a crucial role in the synthesis of higher alcohols from syngas.

Keywords: Perovskite; La(Co, Cu)O_3; High dispersion; CO hydrogenation; Co–Cu metals

1. Introduction

Perovskites are mixed oxides with the formula ABO_3, where B is a small transition metal cation and A is a larger *s*-, *d*-, or *f*-block cation [1]. In the perovskite structure, the *B*-site locates at the center of an octahedron of oxygen ions, and the perovskite unit cell is built from corner-sharing BO_6 octahedra that are connected through B–O–B linkages. The *A*-site occupies the center of eight corner-sharing $BO_{6/2}$ octahedra [2]. Therefore, the B–B distance in framework is relatively large (about 4 Å), so that perovskite has enough space for small molecules (CO, NO_x, CH_4, etc.) to interact selectively with only one transition metal surface ion [3]. Moreover, a large number of metallic elements are stable in the perovskite structure, if their radii satisfy the tolerance factor $t = (r_A + r_O)/\sqrt{2}(r_B + r_O)$ [2]. Because of the high stability of perovskite structure, both A or B cation can be partially replaced by other elements, resulting in numerous derived perovskites having several interesting physical chemical properties [1–3]. For example, the partial substitution at the *A*-site usually leads to the appearance of abnormal oxidation states of the *B*-sites and the formation of structural defects [2,4,5]. Meanwhile, the partial replacement at the *B*-sites results usually in a modification in catalytic activity for some desired catalytic applications [2,3,6]. Lima and Assaf [6] observed that the addition of iron to $LaNiO_3$ perovskite led to the improvement of

*Corresponding author. Fax: +1 418 656 3810.
E-mail address: Serge.Kaliaguine@gch.ulaval.ca (S. Kaliaguine).

0022-4596/$ - see front matter © 2007 Elsevier Inc. All rights reserved.
doi:10.1016/j.jssc.2007.11.016

catalytic stability and an increased resistance to carbon deposition during the methane reforming. Under reduction conditions, nickel and part of the intra-perovskite lattice iron are reduced to metals and form Ni–Fe alloys. This may create a novel pathway to prepare highly dispersed alloys of two transition metals over the sesquioxides Ln_2O_3 by reduction of $LnBB'O_3$ (B' = transition metals) [7,8]. In recent years, there has been an interest in using mixed-oxide-type perovskites $Ln(Co,Fe)O_3$ as precursors for preparation of a "metal-on-oxide" solid. Because of the complexity of perovskite system, which often contains mixed valence ions and variable stoichiometry, a transition metal having multiple oxidation states could exhibit numerous different kinds of catalytic sites active for several reactions when pretreated under tailored conditions [2,3,7]. For example, $La(Co,Fe,Ni)O_3$ perovskites upon reduction at high temperature yield a blend of metals, alloys, ions, etc., which were reported to be active for hydrogenation of ethylene [9], partial oxidation of methane to syngas [10], reforming of CO_2 [11], Fischer–Tropsch synthesis [12], alcohol synthesis [13,14]. In some cases, the catalytic activity was found to be related to the intermediate oxidation states of transition metals and the homogeneity of active sites on the surface [10,12,13,15].

The hydrogenation of CO to oxygenates over Co–Cu-based catalysts from syngas has been known for several decades, but the nature of active sites in such catalysts is still a subject of debate [15–19]. In general, both copper and cobalt are necessary for alcohol synthesis and the metallic cobalt was reported to be present either pure or alloyed with copper [20–22]. Meanwhile, both Cu^0 and Cu^+ along with metallic cobalt are in some cases proposed as active components for conversion of syngas into oxygenates [20,21]. However, Blanchard et al. [23] have reported that only the Co^{2+}/Co^0 centers are active for the synthesis of higher alcohols from syngas over Co/Al_2O_3 catalyst. Meanwhile, Sheffer et al. [24] were unable to detect any metallic Co or Cu^+ on the surface of a Cu–Co–Cr mixed-oxide catalyst. The latter authors suggested that the active catalyst is composed of copper particles supported on Co/Cr spinel. Based on these suggestions, the reduction of $LnB(B')O_3$ perovskite under controlled conditions could be expected to produce an ensemble of transition metals having different oxidation states (metals, ions, etc.), which may be the potential active sites for the synthesis of higher alcohols from syngas. Copper-containing perovskites have been studied for oxygenate synthesis from syngas [13]. The substitution of Mn by Cu in $LaMnO_3$ has, for example, been reported to enhance catalytic conversion of hydrocarbons to methanol and a small amount of C_2^+ oxygenates [13]. In this case, copper is assumed as an active metal for the formation of alcohols (mainly methanol), although its active oxidation state is still undetermined. Moreover, such catalysts are much favored for the synthesis of methanol and show a very low selectivity to higher alcohols, because manganese is not a typical catalyst for propagation of hydrocarbon chain of products. This leads to the assumption that a combination of a metal with a high activity in hydrocarbon formation (Fe, Co, Ru) and copper element in the desired perovskite structure could be a promising catalyst precursor for the synthesis of higher alcohols from syngas. Choosing a $La(Co,Cu)O_3$ perovskite may be ideal for development of a novel higher alcohol synthesis catalyst, because cobalt is usually employed in the Fischer–Tropsch synthesis catalysts and is also very stable in lanthanum cobaltite [1,2,7,14]. This present work is set up with the goal of investigating the characteristics of a series of lanthanum cobaltite perovskites, in which Co is substituted by Cu for conversion of syngas into valuable products. Using Co–Cu-based catalyst precursors with perovskite structure not only fulfills the stability requirements but also leads to the formation of finely dispersed and stable metal particles by the controlled reduction of *B*-site cations in the structure [2,6,7,10,14]. A set of nanocrystalline $La(Co,Cu)O_3$ perovskites prepared by mechano-synthesis have been characterized and pretreated under the same reduction conditions before examining their surface reactivity for the hydrogenation of CO.

2. Experimental

2.1. Perovskite catalyst

$LaCo_{1-x}Cu_xO_{3-\delta}$ ($0 \leqslant x \leqslant 0.3$) perovskites (GM) were synthesized by the reactive grinding method as described in detail in Refs. [14,25]. The oxide precursors including lanthanum, copper, and cobalt oxides with purity of 99^+% (Aldrich) were blended together in stoichiometric proportions. Using a steel crucible and balls usually leads to some minor iron contamination [14,25]. A typical charge of 5 g blended raw materials together with three hardened steel balls of 11 mm diameter was charged in a 50 ml hardened steel crucible. Then, the crucible was sealed under air and fixed on the mill arm. An O-ring was placed between the crucible and the screw cap in order to keep the crucible hermetically closed. A SPEX high-energy ball mill operating at 1000 rpm was used for mechano-synthesis. Milling has been carried out for 8 h. In the second milling step with additives, the resulting powder was mixed with 50% NaCl (99.9%) and further milled for 12 h under the same conditions in order to reach a better dispersion and higher specific surface area. Two leaching operations were performed in order to remove the additive. The slurry was then dried and calcined at 250 °C for 2 h.

Two reference samples, $LaCoO_3$ and $LaCo_{0.7}Cu_{0.3}O_{3-\delta}$, designated as CIT0 and CIT3, respectively, were prepared by the conventional citrate method [13]: a stoichiometric amount of $La(NO_3)_3$ was added into distilled water while slowly heating the mixture on a magnetic stirrer. After a clear transparent solution was obtained, stoichiometric amounts of cobalt and copper nitrates were added. Then, 1 mol of citric acid per mole of metal atom was added to the dark pink/red translucent solution. The resulting solution was heated slowly to dryness and then dehydrated

at 110 °C overnight in a vacuum oven to yield an amorphous solid precursor. The sample was calcined at 800 °C for 6 h with a ramp of 3 °C/min under air. For the synthesis of two mixed oxides of 10 wt% Co_3O_4/La_2O_3 and 10 wt% CuO/La_2O_3 prepared from their corresponding oxides, a mixture of Co_3O_4 (CuO) and La_2O_3 oxides was added into a beaker containing 250 ml of water and stirred by magnetic stirring for 90 min. The slurry was then evaporated in oven at 90–120 °C.

2.2. Characterization

The chemical analysis (Fe, Co, Cu, Na) of the perovskites and the residual impurities was performed by atomic absorption spectroscopy using a Perkin-Elmer 1100B spectrometer. Prior to each analysis, an exact amount of sample was digested in 10% HCl solution at 60–70 °C overnight. The specific surface area of all obtained samples was determined from nitrogen adsorption (BET method) isotherms recorded at −196 °C using a computer-controlled sorption analyzer (OMNISORB 100). 100–300 mg of each sample was degassed at 200 °C for 6–8 h to remove the humidity prior to N_2 adsorption measurements.

Phase analysis and particle size determination were performed by powder X-ray diffraction (XRD) using a SIEMENS D5000 diffractometer with Cu$K\alpha$ radiation ($\lambda = 0.15406$ nm). Bragg's angles between 15° and 75° were collected at a rate of 1°/min. Average crystal domain sizes (D) were evaluated by means of the Debye–Scherrer equation $D = K\lambda/\beta\cos\theta$ after Warren's correction for instrumental broadening [26].

Temperature-programmed reduction (TPR) and temperature-programmed oxidation (TPO) experiments were carried out using a multifunctional catalyst testing and characterization apparatus (RXM-100, Advanced Scientific Designs, Inc.). The reactor was connected to a quadrupole mass spectrometer (UTI 100) and a thermal conductivity detector (TCD). Prior to each TPR analysis, a 40–50 mg sample was calcined for 90 min under flowing 20% O_2/He (20 ml/min, ramp = 5 °C/min) at 500 °C. Then, the sample was cooled down to room temperature under flowing pure He (20 ml/min). TPR profile of the catalyst was then recorded by ramping under 5 vol% of H_2/Ar (20 ml/min) from room temperature up to 800 °C (5 °C/min). The hydrogen consumption was determined using a TCD with a reference gas of the same composition as the reducing gas (H_2/Ar). The effluent gas was passed through a cold trap (dry ice/ethanol) to remove water prior to the detector. For a TPO experiment, a 40–80 mg sample was first calcined at 300 °C for 90 min under flowing 20% O_2/He (20 ml/min, ramp = 10 °C/min). Then, the sample was cooled down to room temperature under flowing pure He (20 ml/min) for 2–3 h. The pretreatment was carried out by ramping under 5 vol% of H_2/Ar (20 ml/min) from room temperature up to 800 °C (10 °C/min) before passing helium (20 ml/min) for 2 h in order to remove adsorbed hydrogen. The TPO experiment was performed by ramping under 20 ml/min O_2/He (5 vol%) from room temperature to 800 °C (5 °C/min).

Temperature-programmed surface reaction (TPSR) of the reduced samples chemisorption of CO with H_2 was carried out on the RXM-100 system. 70–90 mg of the sample was calcined at 500 °C for 120 min under flowing 20% O_2/He (20 ml/min, ramp = 10 °C/min). Then, the sample was cooled down to room temperature under 20 ml/min of helium for 2–3 h. Sample pretreatment was carried out by ramping 10 °C/min under 5 vol% of H_2/Ar (20 ml/min) from room temperature up to 750 °C before passing helium flow (20 ml/min) for 2 h in order to remove adsorbed hydrogen. Then, the reduced forms were performed by flowing 10 ml/min of CO at room temperature for 30 min before switching to the flow of He (20 ml/min) for 15 min. H_2-TPSR measurements were performed under 20 ml/min of H_2 from room temperature to 750 °C (ramp = 10 °C). The effluent gas was led to a quadrupole mass spectrometer (UTI 100). The signals of $m/z = 15$, 16, 18, 28, 30, 32, 41, 42, 44, 46 were collected to monitor the surface reaction.

Temperature-programmed surface reaction (TPSR) with H_2/CO was carried out on the RXM-100 system. 70–80 mg of the sample was calcined at 500 °C for 90 min under flowing 20% O_2/He (20 ml/min, ramp = 10 °C/min). Then, the sample was cooled down to room temperature under 20 ml/min of helium for 2–3 h. Sample pretreatment was carried out by ramping at 5 °C/min under 5 vol% of H_2/Ar (20 ml/min) from room temperature up to 750 °C before passing helium flow (20 ml/min) for 2 h in order to remove adsorbed hydrogen. TPSR measurement was performed by flowing 50 ml/min of a mixture of H_2/CO/He with a ratio of 2:1:22 through the sample while temperature is raised from room temperature to 500 °C (5 °C/min). The effluent gas was led to a quadrupole mass spectrometer (UTI 100). The signals of $m/z = 16$, 26, 30, 32, 41, 42, 44, 46, 56, 58, 60, 74 were collected to monitor the surface reaction between hydrogen and carbon monoxide under atmospheric pressure.

The hydrogenation of CO was run in a stainless-steel continuous-flow fixed-bed micro-reactor (BTRS-Jr PC, Autoclave Engineers). The reaction pressure was controlled using a back-pressure regulator. A mixture of syngas (H_2/CO = 2:1, Praxair) and nitrogen was supplied from a pressurized manifold *via* individual mass flow controllers. The catalyst particle size was 40–60 mesh. Catalysts were pretreated *in situ* under flowing 5 vol% of H_2/Ar (20 ml/min) prior to each reaction test. The temperature was maintained at 250 °C for 3 h and at 500 °C for 3 h with a ramp of 2 °C/min. Then, the reactor was cooled down to the reaction temperature while pressure was increased to 1000 psi by feeding inert gas before switching to the reaction mixture. Butane/helium (4.98 vol%) was used as an internal calibration standard. The products were analyzed using a gas chromatograph equipped with two capillary columns and an automated online gas-sampling

valve maintained at 170 °C. The temperature of transfer line between the reactor and the valves was kept at 220 °C in order to avoid any product condensation. Carbon monoxide and carbon dioxide were separated using a capillary column (Carboxen^{TM} 1006 PLOT, 30 m × 0.53 mm) connected to the TCD. Quantitative analysis of all organic products was carried out using a second capillary column (WCOT fused silica, 60 m × 0.53 mm, coating CP-Sil 5CB, DF = 5.00 μm) connected to an FID detector (Varian CP-3800) and mass spectrometer (Varian Saturn 2200 GC/MS/MS).

3. Results and discussion

3.1. Characterization

The main characteristics of $LaCo_{1-x}Cu_xO_3$ perovskites are reported in Fig. 1 and Table 1. All samples show similar XRD patterns. They are consistent with the pattern described as rhombohedral perovskite structure in JCPDS card nos. 71-0872, 48-0123. However, the XRD spectra of the ground perovskites always show some weak reflection lines of minor Co_3O_4 and CuO oxides. Meanwhile, although the substitution for cobalt by copper is prepared up to 30%, traces of segregated single copper oxide phase characterized by two strong reflections at $2\theta = 35.7°$ and 38.9° are clearly observed with sample CIT3 prepared by the citrate complex recipe. Therefore, a noticeable amount of copper ions is still located out of the perovskite lattice. Fig. 1 also reveals that the peak width of all ground perovskites is much broader than those of the citrate-derived samples. This implies that the crystal domain sizes of the former samples (GM) are much smaller than those of the latter ones (CIT). As estimated by the Debye–Scherrer equation, average crystal domain sizes of the ground perovskites are about ~10 nm (Table 1). These are in accordance with the observations of SEM photographs (not shown here) and our previous findings [14,25,27].

Table 1 shows that the ground perovskites always retain a small amount of remnant alkali, which may cause a small

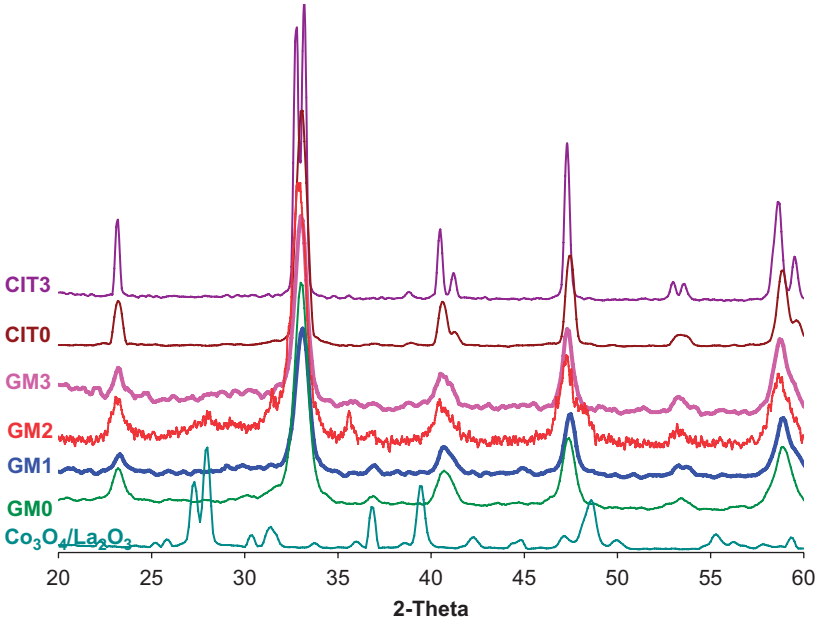

Fig. 1. XRD spectra of $LaCo_{1-x}Cu_xO_3$ perovskites and Co_3O_4/La_2O_3.

Table 1
Physical properties of La(Co,Cu)O_3

Sample	Perovskite	Recipe	Na^+ (wt%)	Calcination temperature (°C)	Surface area (m^2/g)	Crystal domain size (nm)[a]
GM0	$LaCoO_3$	Grinding	0.53	250	59.6	9.8
GM1	$LaCo_{0.9}Cu_{0.1}O_3$	Grinding	0.31	250	19.5	9.7
GM2	$LaCo_{0.8}Cu_{0.2}O_3$	Grinding	0.08	250	28.1	9.3
GM3	$LaCo_{0.7}Cu_{0.3}O_3$	Grinding	0.17	250	22.3	9.9
CIT0	$LaCoO_3$	Citrate	–	600	1.2	32
CIT3	$LaCo_{0.7}Cu_{0.3}O_3$	Citrate	–	800	4.7	>35

[a]Calculated using the Scherrer equation from X-ray diffraction line broadening.

loss in surface area. The surface area of all Cu–Co-based perovskites (GM1–GM3) is fairly lower than that of the copper-free catalyst (GM0), but still much higher than the ones of the citrate-derived samples (CIT0–CIT3). This is indeed related to the low synthesis temperature during reactive grinding [25]. The substitution of Co^{3+} with Cu^{2+} in perovskites has led to a decline in the surface area of lanthanum cobaltite from 60 to 20–30 m^2/g, in spite of similar preparation conditions.

3.2. Temperature-programmed reduction (TPR)

3.2.1. $LaCoO_3$

The reducibility of $LaCoO_3$ perovskites was investigated by TPR by hydrogen. H_2-TPR performance was carried out from room temperature to 800 °C. Fig. 2 presents two H_2-TPR curves of Co-based perovskites prepared by two different recipes and Co_3O_4/La_2O_3 reference. Unlike the reduction of Co_3O_4/La_2O_3 that occurs at 350–400 °C, $LaCoO_3$ is reduced over the temperature range of 250–750 °C and through a multiple-step process [1,2,7,8,10,11,28]. As seen from Fig. 2, H_2-TPR curve of the ground Co-based perovskite (GM0) shows two very large peaks with some small shoulders, while that of the citrate-derived $LaCoO_3$ sample (CIT0) displays two clearly shaped peaks. The former sample (GM0) starts reducing at a lower temperature, but finishes at a higher reduction temperature. The H_2 balance indicates that the low-temperature region (200–450 °C) is assigned to the reduction of Co^{3+} to Co^{2+} [7,9,28,29]. In order to investigate the thermal structural stability as well as the reduction steps of the ground $LaCoO_3$ perovskite under this reduction condition, XRD spectra of $LaCoO_3$ sample (GM0) reduced at different temperatures were collected. Fig. 3 shows that the structure of $LaCoO_3$ is essentially unchanged in the low-temperature range of 200–400 °C.

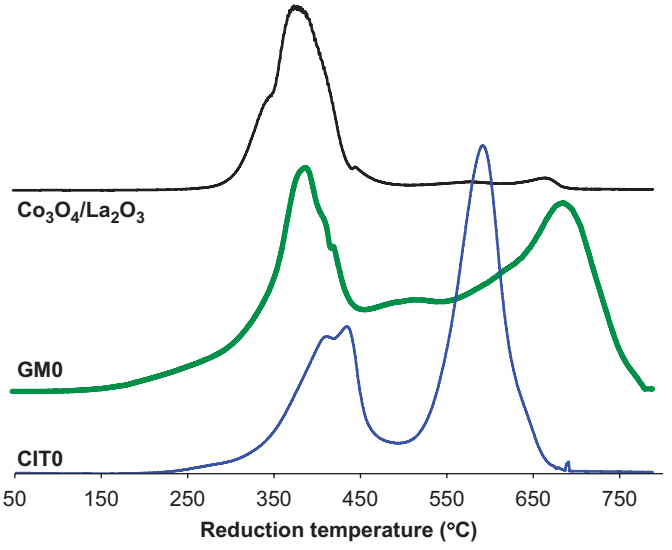

Fig. 2. H_2-TPR profiles of $LaCoO_3$ perovskites and 10 wt% Co_3O_4/La_2O_3.

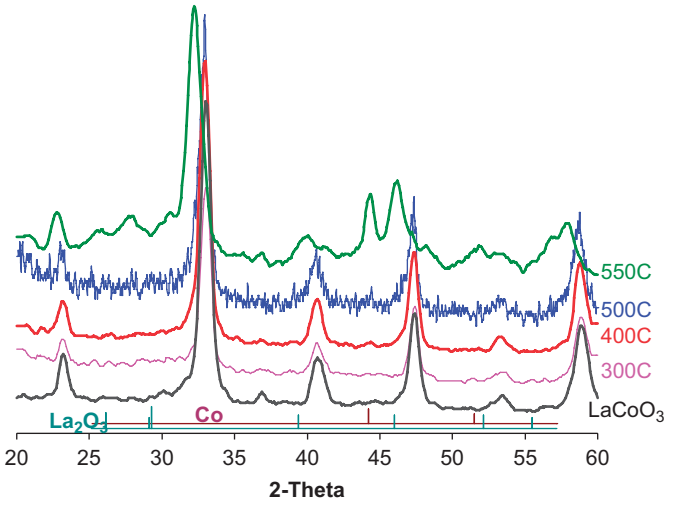

Fig. 3. XRD spectra of GM0 ($LaCoO_3$) reduced at different temperatures (20 ml/min of 5 vol% H_2/Ar) and sintered at $T_{reduction} = 25$ °C under 20 ml/min of helium for 90 min.

Therefore, the first peak is definitely attributed to the reduction step [7,8,28]:

$$LaCoO_3 + xH_2 \rightarrow LaCoO_{3-x} + xH_2O \quad (1)$$

where x is close to 0.5, which would correspond mainly to the reduction of Co^{3+} to Co^{2+} [7,27,29]. The corresponding TPR peak shifts to a higher temperature from sample $LaCoO_3$ (GM0) (387 °C) to $LaCoO_3$ (425 °C) (CIT0). The lower reduction temperature observed with sample GM0 is presumably caused by an effect of the higher specific surface area (see Table 1). A ground perovskite is usually composed of agglomerates of elementary nanometric particles and its porous structure is formed by clustering the primary particles, as clearly indicated in several previous reports [14,25,27,29]. Therefore, in addition to the higher rate of the surface process, the diffusion of H_2 and the mass transport of H_2O across lattice of the porous ground perovskite (GM0, $S_{BET} = 59\ m^2/g$) become much easier than those of the citrate-derived perovskite (CIT0, $S_{BET} = 1.2\ m^2/g$), which has essentially no porosity [2,7,8,10,12,29,30].

The high-temperature peak (500–780 °C) along with some visible shoulders is attributed to only the reduction of Co^{2+}/Co^0 because the reduction of La^{3+} to lower oxidation states requires a higher temperature [2,7,8,28]. As seen from Fig. 2, both the low- and high-temperature peaks are rather broadened, indicating the existence of certain different Co^{3+} species on the surface or in the grain boundaries of the ground lanthanum cobaltite [7,10,29–31]. As reported earlier in Refs. [14,25,29], the ground perovskites always give a rather high surface area and have many grain boundaries. They show more oxygen vacancies present in the bulk as well as low coordination cobalt ions on the surface [7,25,27,29]. As a result, a part of cobalt ions in the grain boundaries are more reducible. Indeed, the XRD pattern of $LaCoO_3$ (GM0) reduced at 500 °C shows some weak reflections of Co^0 at $2\theta = 44.4°$

and 51.5° (Fig. 3), but these are more intense at the reduction temperature of 550 °C. In the latter case, the perovskite structure is strongly modified with the appearance of diffraction lines of La_2O_3. This demonstrates that part of the perovskite was destroyed and cobalt formed on the surface catalyst in metallic form is stabilized by the perovskite lattice under these experimental reduction conditions (⩽550 °C).

3.2.2. *La(Co,Cu)O₃*

H_2-TPR profiles of La(Co,Cu)O_3 samples are similar to that of lanthanum cobaltite perovskite as displayed in Figs. 2 and 4. Two main peaks are present in H_2-TPR spectra of Cu-containing perovskites. Compared with the data of CuO/La_2O_3 reduction under the same experimental conditions, the low-temperature region in H_2-TPR traces of La(Co,Cu)O_3 perovskites is attributed to the simultaneous reduction of both Cu^{2+}/Cu^0 and Co^{3+}/Co^{2+} [32]. Indeed, the XRD spectrum of the representative $LaCo_{0.7}Cu_{0.3}O_3$ sample (GM3) reduced at 375 °C and sintered at 350 °C for 90 min under helium confirms this suggestion. Fig. 5 shows some diffraction lines characterizing the presence of metallic copper but no clear reflections of metallic cobalt. Simultaneously, no significant changes in the diffraction line positions between the incompletely reduced form and the fresh sample GM3 are observed, but very strong broadening peaks and in some lines a splitting are shown under the reduction conditions reported in Fig. 5. These demonstrate that the perovskite structure is still kept and copper atoms are assumedly well dispersed in the perovskite framework at the end of the first reduction stage (Fig. 4). Fig. 4 also reveals that the intra-lattice copper ions are reduced at a higher temperature, whereas the reduction of cobalt ions takes place at a lower one, in comparison with those of corresponding oxides (Figs. 2 and 4). Moreover, an increased copper content results in a systematic shift of the first reduction peak to lower temperatures. This is caused by the close vicinity and electronic interaction between Cu^{2+} and Co^{3+} sites in the perovskite lattice. The reduced copper has promoted the reducibility of neighboring cobalt ions, apparently by providing activated hydrogen [14,33]. Fig. 4 also indicates that the high-temperature peak is likely independent of the amount of the intra-perovskite lattice copper, but it is essentially at a lower temperature than that of lanthanum cobaltite perovskite. Thus, the reductive pretreatment of the ground La(Co,Cu)O_3 perovskites carried out a relatively low temperature (450–550 °C) and kept in isothermal reduction conditions allows to produce a high dispersion of Co, Cu metals and avoids the sintering of their metallic particles [14,29]. The copper cobalt metals formed this way may show extraordinary catalytic activity in the hydrogenation of CO [9,10,12,14,15] because they are either so finely dispersed in the resulting matrix La_2O_3 or atomically stabilized in the perovskite framework [8,12,29]. The complete reduction of cobalt ions accompanied by the collapse of the perovskite structure occurs at 750–800 °C. XRD spectrum of sample GM3 reduced at 800 °C followed by sintering at 775 °C under 20 ml/min of helium shows two typical reflections of metallic cobalt at $2\theta = 44.38°$ and 51.47° (Fig. 5) in addition to signals of La_2O_3. This demonstrates the formation of a high surface area of metals extracted from the perovskite framework.

In order to shed light on the effect of preparation conditions and pretreatment variables on the redox behavior and the stability of nanocrystalline La(Co,Cu)O_3 perovskites, numerous TPR experiments of $LaCo_{0.7}Cu_{0.3}O_3$ sample were tested as functions of calcination temperature and the amount of remnant additive (Na^+)

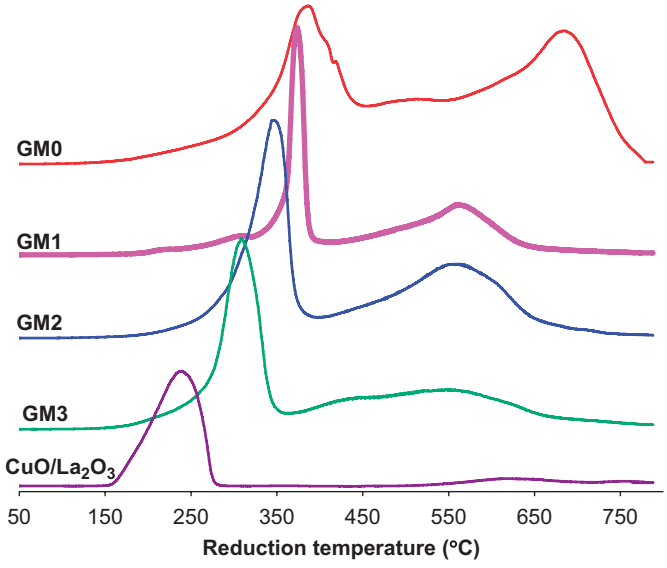

Fig. 4. H_2-TPR profiles of $LaCo_{1-x}Cu_xO_3$ perovskites and 10 wt% CuO/La_2O_3.

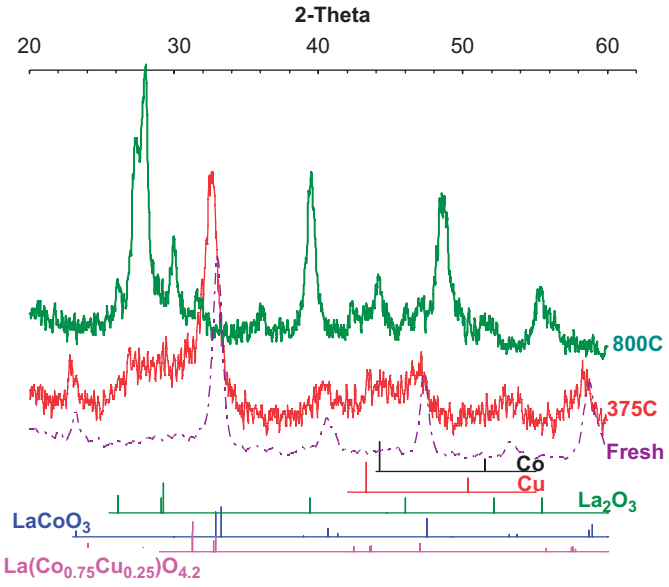

Fig. 5. XRD spectra of GM3 ($LaCo_{0.7}Cu_{0.3}O_3$) pattern reduced at 375 and 800 °C (20 ml/min of 5 vol% H_2/Ar, ramp = 5 °C/min) and sintered at 350 and 775 °C, respectively, under 20 ml/min of He for 90 min.

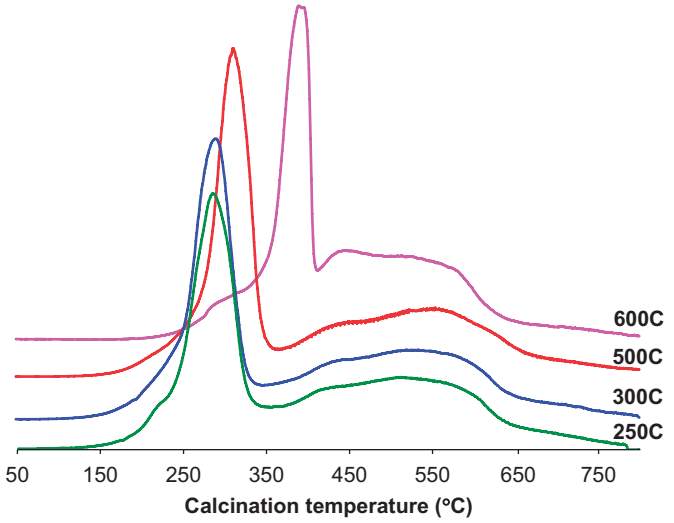

Fig. 6. H_2-TPR profiles of GM3 ($LaCo_{0.7}Cu_{0.3}O_3$) perovskite calcined at different temperatures (20 ml/min of 20 vol% O_2/He, ramp = 5 °C/min).

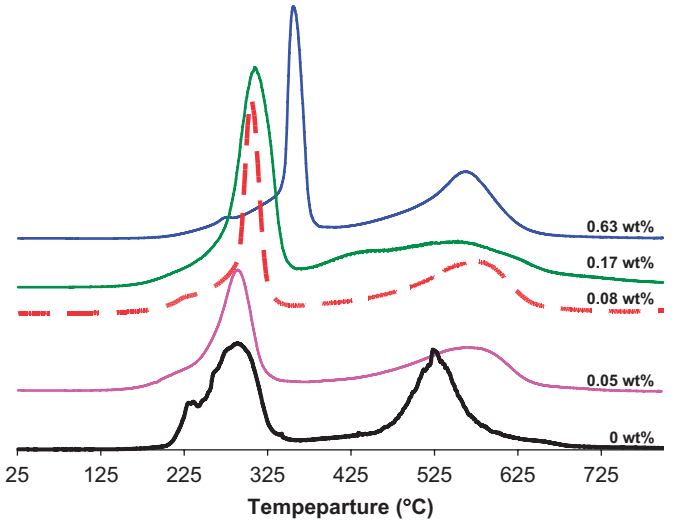

Fig. 7. H_2-TPR profiles of GM3 ($LaCo_{0.7}Cu_{0.3}O_3$) at different amounts of remnant Na^+ (the 0.0 wt% refers to sample prepared by the citrate complex method).

[14,25]. The results are shown in Figs. 6 and 7. As seen from Fig. 6, the low-temperature peak clearly moves to a higher reduction temperature, while the second peak is almost unaffected as calcination temperature increases. This is associated with the sintering process that causes a decreased external surface area and produces a narrower crystal size distribution with a higher mean crystal domain size as the catalyst is treated at a higher temperature. In addition, the ground perovskite surface comprises a large concentration of OH groups because of preparation at a rather low temperature (~40 °C) [25]. These hydroxyls are eliminated during the calcination process, leading to the reformation of perovskite lattice and a drastic decrease in specific surface area as well as a change in the pore system [25,34]. Consequently, the increased diffusional resistance results in an observable shift of the low-reduction temperature peak to a higher level in H_2-TPR trends [8,10,25,29,34–36]. H_2-TPR results in Fig. 6 reveal that the effect of pretreatment temperature on the reducibility of the ground perovskites is negligible if the sample is precalcined below 500 °C.

All ground $La(Co,Cu)O_3$ perovskites usually contain a small amount of remnant alkali added during the preparation (Table 1) [14,25,37]. The presence of residual additive affects not only the specific surface area but also the reducibility of the transition metal at *B*-sites. Fig. 7 shows the changes in reduction temperature of Co^{3+} and Cu^{2+} with the amount of remnant sodium ions. In the absence of alkali additive, the citrate-derived sample shows two principal peaks with a visible shoulder at ~235 °C. This shoulder is firmly assigned to the reduction of the extra-perovskite lattice copper, in harmony with the H_2-TPR result of CuO/La_2O_3 reported in Fig. 4. As seen from Fig. 7, no significant differences in low-temperature H_2-TPR curves between samples retaining a very small amount of sodium ions below 0.1 wt% are observed. At a higher content of remnant Na^+, the reduction peak of Cu^{2+}/Co^0 and Co^{3+}/Co^{2+} (low-temperature region) clearly shifts to a higher temperature, while the reduction temperature of Co^{2+}/Co^0 changes insignificantly. This indicates that the first reduction step of the ground $La(Co,Cu)O_3$ perovskites is remarkably affected by the presence of basic ions as well as any change in the catalyst surface (Figs. 6 and 7) [25,34,37–40]. At higher content, residual sodium ion makes a decreased surface area, blocks surface Co–Cu atoms and inhibits reduction of Cu^{2+}, Co^{3+} to lower oxidation states [33,38,40].

3.3. Temperature-programmed oxidation (TPO)

In order to investigate the re-oxidation of the reduced perovskite, O_2-TPO experiments of some representative Co–Cu-based samples were carried out under 20 ml/min of O_2/He (20 vol%) after running H_2-TPR up to 800 °C (Fig. 5). In agreement with H_2-TPR results, O_2-TPO profiles show the re-oxidation of the reduced perovskites occurring in two steps (Fig. 8) [10]. The first process takes place in the temperature range of 100–400 °C. A careful quantitative analysis of oxygen balance indicates both metallic cobalt and copper being oxidized to higher oxidation states by reactions (2) and (3):

$$Cu^0 + \tfrac{1}{2}O_2 \rightarrow CuO \quad (2)$$

$$Co^0 + \tfrac{2}{3}O_2 \rightarrow \tfrac{1}{3}Co_3O_4 \quad (3)$$

It is noted here that the onset temperature for the oxidation of all ground perovskite precursors is rather low and the low-temperature peak is very large. Meanwhile, the window temperature for the partial oxidation of metallic cobalt, copper in the case of the citrate-derived perovskite precursors is appreciably narrower (Fig. 8). This is consistent with the H_2-TPR results and explained by the

differences in catalyst morphology between the two kinds of perovskites (GM0 and CIT0) studied here.

The high-temperature peak (590–650 °C) is attributed to the second oxidation step corresponding to the formation of La–Co perovskite. In this step, the rest of Co^{2+} is oxidized to Co^{3+} simultaneously with a solid-state reaction to restore the perovskite structure for sample GM0. Fig. 9a shows a well-crystallized rhombohedral structure of the regenerated $LaCoO_3$ perovskite (GM0) after running TPO up to 800 °C. These results suggest that a high dispersion of metallic cobalt was formed after the complete reduction of $LaCoO_3$ [8,9,21], so that the re-oxidation of this sample can easily reproduce the original perovskite structure (Fig. 9a) [8,10]. In contrast, the re-oxidation of the reduced Co–Cu-based perovskite (GM3) is much less reversible. The X-ray spectrum of the re-oxidized Co–Cu sample reflects the presence of a mixture of phases (Fig. 9b). One of these presents the $LaCo(Cu)O_3$ perovskite crystal structure and the others are some La_2O_3, Co_3O_4, CuO crystallites, indicating an incomplete regeneration of the reduced ground $LaCo_{0.7}Cu_{0.3}O_3$ sample (GM3). This is interpreted by the fact that at a high temperature (800 °C), copper oxides tend to agglomerate into larger particles that prevent the solid-state reaction between oxide particles. Therefore, the re-oxidation in this case did not completely regenerate the parent phase (Fig. 9b). This is in agreement with the results of Porta et al. [31], who indicated some difficulties in preparing a single phase of the copper-poor perovskite $LaCo_{1-x}Cu_xO_3$ ($x \leqslant 0.2$) at a high calcination temperature ($\geqslant 800$ °C) under oxygen atmosphere. These observations suggest that nanocrystalline Co–Cu-based perovskites with a higher copper content ($x \geqslant 0.3$) synthesized at low temperature using reactive grinding method may be particularly well suited to prepare a supported bimetallic catalyst having well dispersed cobalt copper metals.

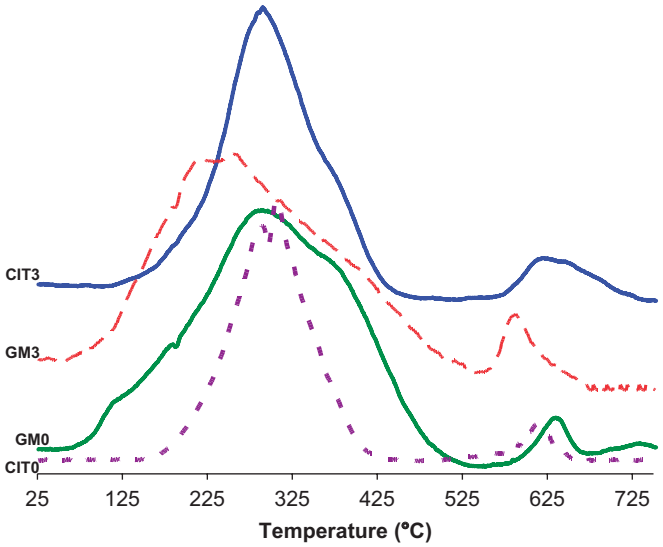

Fig. 8. O_2-TPO curves of $LaCo_{1-x}Cu_xO_3$ perovskites.

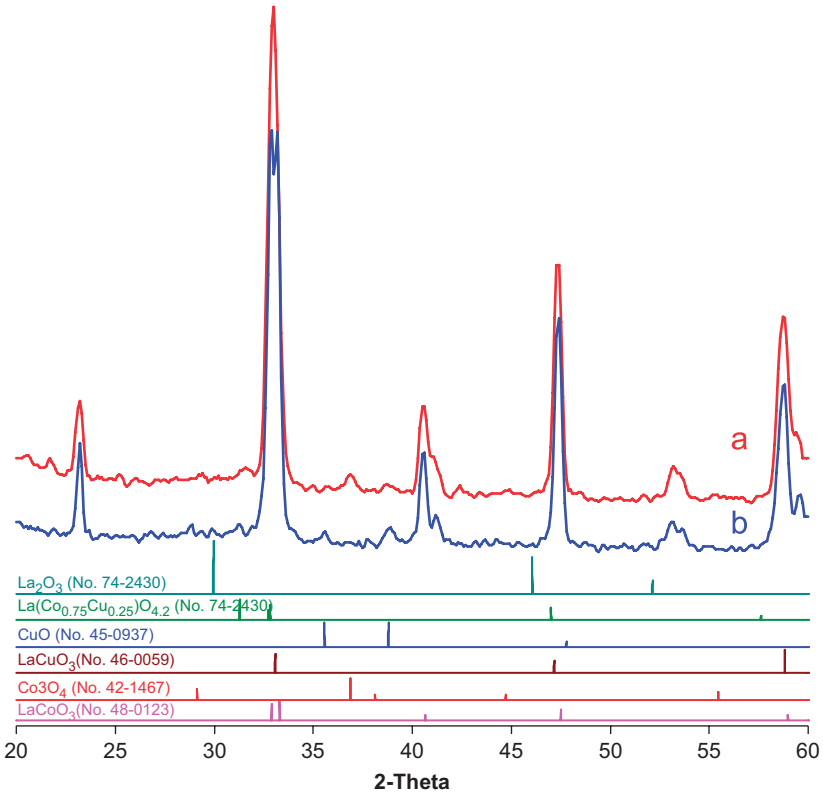

Fig. 9. XRD spectra of GM0 ($LaCoO_3$) (a) and GM3 ($LaCo_{0.7}Cu_{0.3}O_3$) (b) after O_2-TPO measurement at 800 °C.

3.4. Temperature-programmed surface reaction (TPSR)

3.4.1. TPSR of chemisorbed CO with H_2

The reactivity of chemisorbed CO under H_2 flow can provide useful information about the ability of Co–Cu metal surface to dissociate and to hydrogenate the carbon monoxide molecule. Because the hydrogenation of carbon into methane usually takes place very fast on Co-based catalysts, the formation of methane is considered as a useful indication in the investigation of CO dissociation on the catalyst metal surface. Three ground perovskites (GM0–GM3) were reduced at 750 °C before adsorption of CO at room temperature. Fig. 10 shows the production of CH_4 when hydrogenation of chemisorbed CO on the reduced perovskites was performed from room temperature to 750 °C (ramp = 10 °C/min) under 20 ml/min of H_2. For the copper-free perovskite sample (GM0), a methane signal was found at rather low temperature (~165 °C) and reached two maxima at temperatures of 230 and 430 °C, but sharply increased at a temperature higher than 650 °C. According to literature [41–43], the low-temperature peak is attributed to the formation of methane from the hydrogenation of atomic carbonaceous species resulting from the dissociative adsorption of CO on large ensembles of cobalt atoms. The 230 °C peak is assigned to methane formed through the decomposition of either $(CH_x)_nO$ or polymerized $(–CH_x–)_{n=2–3}$ species adsorbed on metallic particles under atmospheric pressure. Methane signals detected at higher temperatures (>650 °C) are reported to come from the hydrogenation of carbide surface [42]. As copper inserts into the perovskite lattice, three effects are observed. Firstly, the absence of the lower temperature peak (⩽230 °C) suggests that cobalt atoms seem to be alloyed with Cu atoms to form Co–Cu bimetallic particles [41]. Secondly, the temperatures at which the signal of methane appears and the corresponding maximum were shifted to higher temperatures (Fig. 10). The other effect is a significant decrease in area of the high-temperature (>650 °C) methane peak, reflecting the disappearance of some active sites responsible for the formation of this product [44,45]. This latter result may indicate that the presence of copper in the reduced metallic phase prevents the formation of carbide.

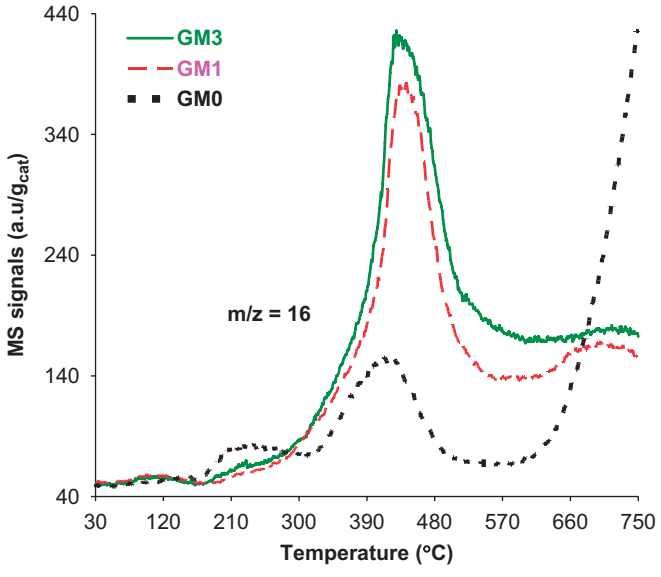

Fig. 10. CH_4 traces in H_2-TPSR spectra of reduced La(Co,Cu)O_3 after chemisorption of CO at room temperature.

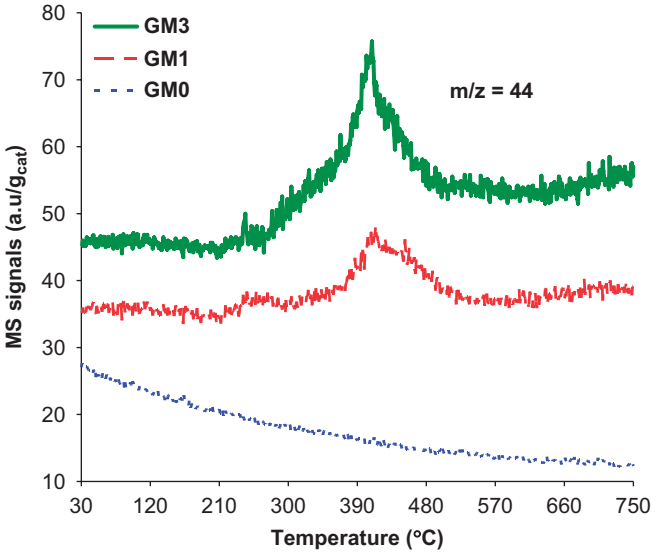

Fig. 11. CO_2 traces in H_2-TPSR spectra of reduced La(Co,Cu)O_3 after chemisorption of CO at room temperature.

Under these experimental conditions, no peaks of CO_2 were observed over the ground $LaCoO_3$ precursor, but small peaks were found at 420 °C over the ground Co–Cu-based samples GM1 and GM3 (Fig. 11).

3.4.2. TPSR with syngas

TPSR experiments on nanocrystalline La(Co,Cu)O_3 samples have been carried out from room temperature to 500 °C under ambient pressure in order to investigate the activity in CO hydrogenation over the reduced perovskites. All m/z-TPSR profiles for the three ground Co–Cu-based perovskite precursors are presented in Figs. 12–16. The appearance in Fig. 12 of MS signals at $m/z = 16$ belonging to methane demonstrates that the catalyst surface provides mainly cobalt sites, which can dissociate the CO molecule followed by hydrogenation of the surface carbon atoms to methane and hydrocarbons [46,47]. Fig. 12 shows that for the three ground $LaCo_{1-x}Cu_xO_3$ perovskites (GM0–GM3) used, the formation of methane increases with increasing temperature. The onset temperature for methane formation over sample GM0 $LaCoO_3$ (220 °C) is much lower than those on catalysts GM1 and GM3 La(Co,Cu)O_3 (250 °C) and shifts toward a higher temperature with increasing copper content, in agreement with the results reported in Fig. 10. This is probably caused by either an electronic interaction between metallic cobalt and neighboring coppers or the formation of Co–Cu alloys [14,48–51],

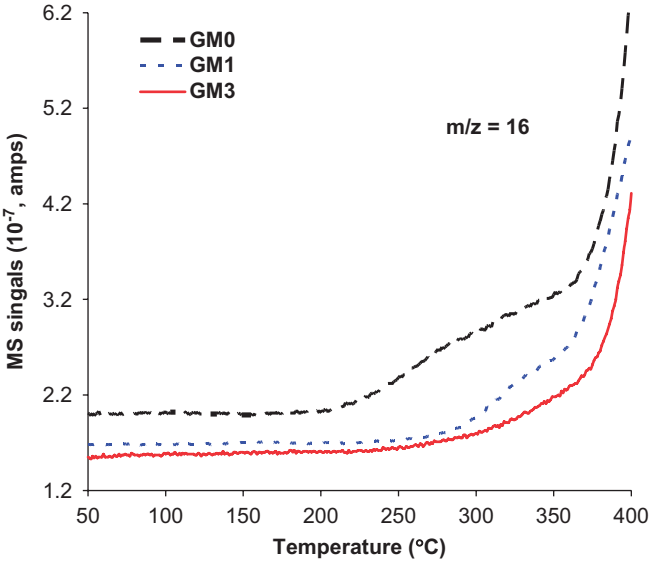

Fig. 12. Methane ($m/z = 16$) profiles during TPSR with H_2/CO/He over $LaCo_{1-x}Cu_xO_3$ reduced at 750 °C.

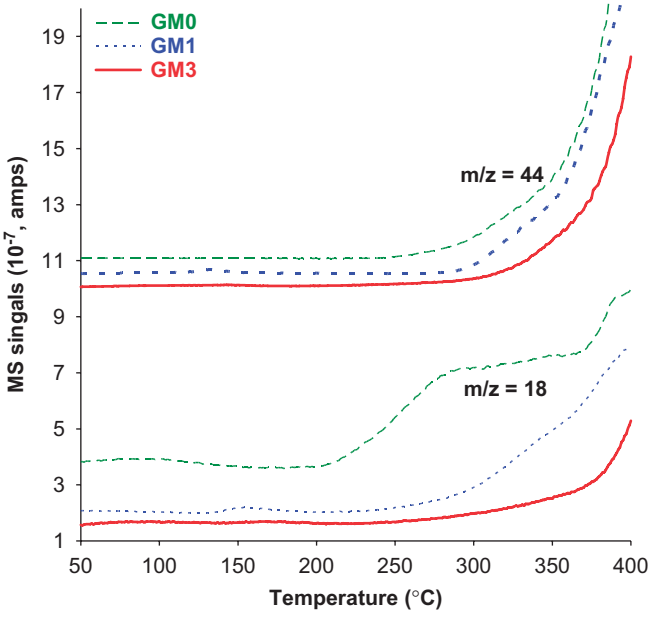

Fig. 13. Carbon dioxide ($m/z = 44$) and water ($m/z = 18$) profiles during TPSR with H_2/CO/He over $LaCo_{1-x}Cu_xO_3$ reduced at 750 °C.

which both resulted in the decreased activity of cobalt in the hydrogenation of intermediates [20,33,52].

Fig. 13 shows the variations in carbon dioxide ($m/z = 44$) and water ($m/z = 18$) during H_2-TPSR of CO with temperature. The curve of water is similar to that of methane, demonstrating that both methane and water are derived from the hydrogenation of C- and O-surface species. For the ground Co-based perovskite (GM0), signal of water gradually increases from 200 to 300 °C and reaches a plateau in the temperature range of 300–375 °C; meanwhile the signal of carbon dioxide begins to stand out at around 300 °C. This indicates that either water formed

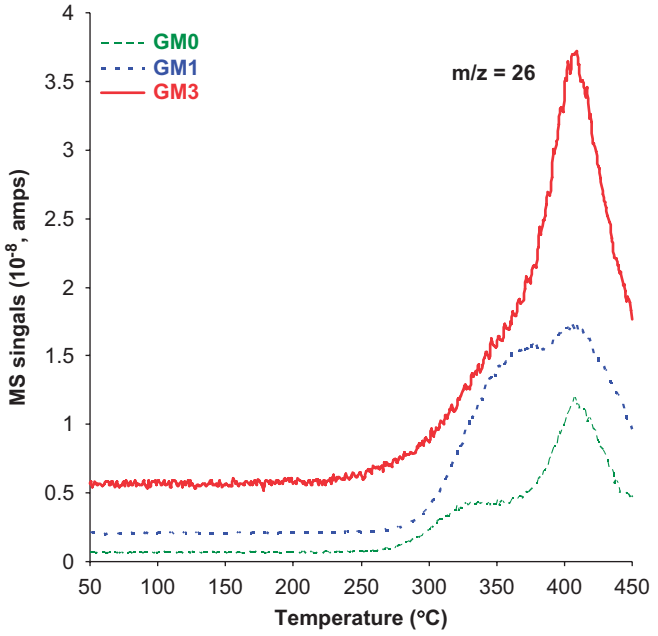

Fig. 14. Signals of $m/z = 26$ during TPSR with H_2/CO/He over $LaCo_{1-x}Cu_xO_3$ reduced at 750 °C.

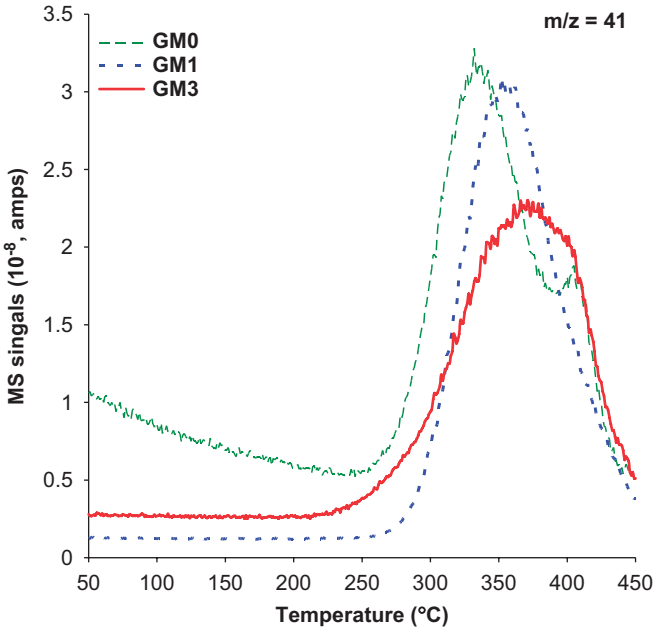

Fig. 15. Signals of $m/z = 41$ during TPSR with H_2/CO/He over $LaCo_{1-x}Cu_xO_3$ reduced at 750 °C.

or O-surface species takes part in the water–gas shift reaction, resulting in the formation of CO_2 [10,43,46,52]. In the case of Co–Cu-based perovskites, a similarity is observed between water and carbon dioxide curves. The formation of water and CO_2 on these catalysts occurs, however, at a higher temperature as compared to the copper-free perovskite (Fig. 13).

Fig. 14 presents the signal of $m/z = 26$ which is assigned to a fragment ion of C_2 ($C_2H_2^+$) hydrocarbons, as a function of temperature. A peak appears at 410 °C along

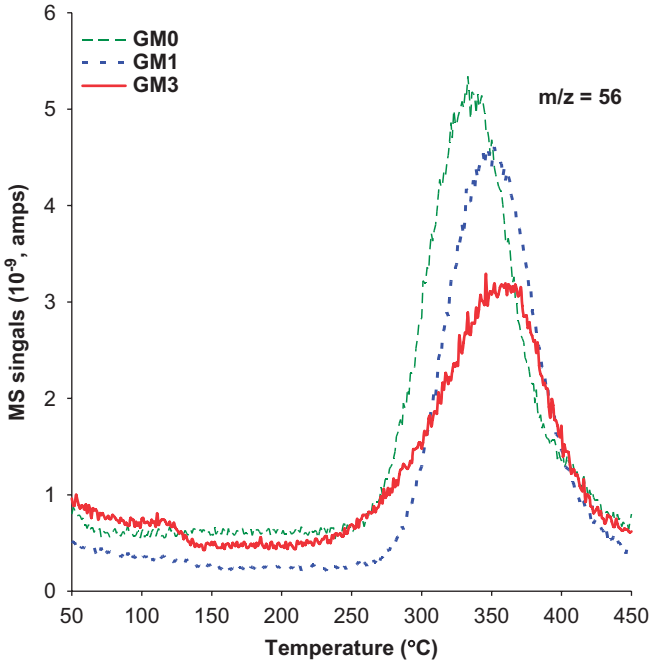

Fig. 16. Signals of $m/z = 56$ during TPSR with H_2/CO/He over $LaCo_{1-x}Cu_xO_3$ reduced at 750 °C.

with a shoulder at 325–350 °C. These fractures are reminiscent of the medium-temperature peaks of desorbed CH_4 shown in Fig. 10. The C_2 hydrocarbons are therefore generated simultaneously with methane. This suggests that the (CH_x) groups are present when the C_2 species are formed and therefore that the hydrocarbon chain propagation involves the insertion of a (CH_x) species in an alkyl intermediate adsorbed on the catalyst surface, which is the generally accepted view [47,52,53]. This is further supported by the essentially simultaneous appearance of $m/z = 41$ and 56 which are related to C_3 and C_4 hydrocarbon species as displayed in Figs. 15 and 16. The signals of products reported in Figs. 12 and 14–16 allow comparing the reactivity of the catalyst surface for CO hydrogenation. The peaks of higher hydrocarbons ($m/z = 41$, 56) shifts to a higher temperature as the copper content increases. Secondly, the reduced $LaCoO_3$ sample tends to produce more methane (and may be more saturated hydrocarbon products) because of a high activity in CO hydrogenation of metallic cobalt [12,47]. Thus, this sample should be modified by either an addition of a small amount of alkali promoters [33,37,46] or the insertion of copper atoms into La–Co–O perovskite lattice [14] in order to diminish the production of undesired gaseous hydrocarbons. The latter assumption is supported by both the data of TPSR presented in Figs. 15 and 16 and the results of CO hydrogenation reported below.

3.5. Hydrogenation of CO

TPSR spectra provide much useful information for the performance of these catalysts in CO hydrogenation reaction. The hydrogenation of CO was tested at 275 °C, 1000 psi, H_2/CO/He = 8:4:3, VVH = 5000 h^{-1} over all Co–Cu-based samples (GM and CIT) and the results are summarized in Table 2. The products comprised linear primary alcohols from methanol to heptanol, small amounts of secondary alcohols, mixtures of normal paraffins, olefins, carbon dioxide, and water, although no observable signals of oxygenated products are shown in TPRS spectra. It is likely that the synthesis of higher alcohols is not favored under the conditions of TPSR measurements namely at ambient pressure and very high velocity [52–54]. Table 2 clearly shows that several complex reactions including alcohol formation, Fischer–Tropsch synthesis, methanation, water–gas shift reaction all take place on the catalyst surface. For the ground perovskite precursors (GM samples), the overall activity increases with increasing copper content in the perovskite lattice. The copper-free perovskite produces mainly hydrocarbons and a small amount of alcohols. Meanwhile, the Co–Cu-based perovskites are more active for alcohol synthesis in spite of yielding a larger amount of methane from $(–CH_x)_nO$ species at ~420 °C (Fig. 10). This indicates that the presence of surface $(CH_x)_nO$ intermediates could be related to the activity in the synthesis of higher alcohols. Instead of being hydrogenated into methane and/or hydrocarbons on cobalt sites, these oxygenate species tend to convert to higher alcohols over cobalt atoms alloying or pairing with copper [14,37,48,49].

CO_2 selectivity expressed as WGS (%) is shown as a function of the overall activity and the amount of copper reported in Table 2. It is known that cobalt-based catalysts are not very active for the water–gas shift reaction [47], which is indeed confirmed by the abundance of water reported in Fig. 13 and the results of H_2-TPSR discussed earlier (Fig. 11). The presence of copper in the perovskite structure promotes the formation of CO_2 through water–gas shift reaction [55]. Meanwhile, no significant differences in activity as well as WGS (%) between the two citrate-derived samples (CIT0 and CIT3) are observed, but the overall activity and alcohol productivity of these catalysts are much lower than those of the corresponding ground perovskites. This can be explained by the differences in catalyst morphology between the two perovskite series prepared by different recipes [13,37]. While the ground perovskites have nanoparticles and a plentiful system of grain boundaries with a high surface-to-volume ratio of nanocrystals, the citrate-derived samples show a rather low specific surface area (Table 1). It should be born in mind that the catalytic reactions mainly take place over the reduced perovskite catalyst surface. Therefore, the differences in selectivity are related to the concentration of surface species, the amount of remnant sodium ions, and the metal surface [54]. The H_2-TPSR of chemisorbed CO shows the catalyst surface comprising various carbonaceous species [41,42]. Their reactivity assigned from the temperature of methanation is affected by the presence of copper on the catalyst surface. Indeed, copper metals

Table 2
Products of CO hydrogenation at 275 °C (1000 psi, 5000 h^{-1}, H_2/CO/He = 8:4:3, excluding CO_2)

Sample		GM0	GM1	GM2	GM3	CIT0	CIT3
Formula		$LaCoO_3$	$LaCo_{0.9}Cu_{0.1}O_3$	$LaCo_{0.8}Cu_{0.2}O_3$	$LaCo_{0.7}Cu_{0.3}O_3$	$LaCoO_3$	$LaCo_{0.7}Cu_{0.3}O_3$
Activity (μmol CO/g_{cat}/h)		63.0	69.8	169.6	188.4	44.5	40.9
WGS (%)		2.13	3.92	5.41	6.59	0.32	0.45
Methane	Selectivity[a]	23.9	17.7	25.3	24.8	49.6	46.7
	Productivity[b]	24.3	20.6	37.8	41.2	71.8	65.0
C_2^+ hydrocarbons	Selectivity[a]	40.9	30.9	33.1	32.3	41.1	39.1
	Productivity[b]	39.1	36.0	44.6	53.4	24.3	20.1
C1–C7 alcohols	Selectivity[a]	19.5	32.8	41.4	44.9	9.3	14.4
	Productivity[b]	21.4	40.0	49.2	60.9	6.3	12.9
$\alpha_{C2–C7\ alcohols}$		0.35	0.47	0.45	0.41	0.31	0.36
$\alpha_{hydrocarbons}$		0.58	0.49	0.46	0.43	0.39	0.37

[a]Unit: wt%.
[b]Unit: mg/g_{cat}/h.

alloying or pairing with cobalt atoms result in a significant decrease in the rate of CO dissociation and the increased stabilization of $(CH_x)_nO$ species. Consequently, the relative surface coverage of CO* and H* (θ_H/θ_C) will change, leading to a change in the overall activity and in the product distribution. Indeed, all ground Co–Cu-based samples produce less methane and more C_2^+ hydrocarbons (Table 2). Under the reported conditions, both alcohol selectivity and productivity increase with increasing copper content, while the formation of methane is likely correlated with the presence of sodium additive and the particle sizes of catalysts. Table 2 shows that methane is the dominant reaction product formed over the two citrate-derived perovskites (CIT0 and CIT3), which have no alkali promoters and larger crystal domain sizes (Table 1). It is well known that a proper amount of alkali ions (Cs, K, Na) over transition metals lowers the work function [54,56], thus enhancing the electron-donation capacity of the surface. During the hydrogenation of CO, when carbon monoxide adsorbs on an alkali ion doped surface, there is a correspondingly large charge exchange between the adsorbed molecule and the Na^+-modified surface. Therefore, the presence of Na^+ leads to an enhancement of the energy of adsorption of CO and the rate of CO dissociation. As a result, the selectivity to methane decreases, while that of both C_2^+ hydrocarbons and higher alcohols increases with the presence of alkali additive. Indeed, the carbon chain growth probability factor of hydrocarbons ($\alpha_{hydrocarbons}$) is found to be higher on all perovskite samples promoted with remnant sodium (samples GM0–GM3) compared with the two citrate-derived catalysts (CIT0 and CIT3). This explains for example the lower activity in higher alcohol synthesis of sample CIT3 which has no alkali promoters compared with GM3 of otherwise same composition. The higher propagation constants of hydrocarbons as well as alcohols (Table 2) correspond to a decreased hydrogenation capacity of the Na^+-modified catalyst surface, which is reasonable since methanation is a reaction competing with chain growth on the surface. This leads to an increased selectivity for longer hydrocarbon-chain products. As indicated by H_2-TPR data and XRD spectra, the reduced ground perovskites contain both copper and cobalt in metallic form over the Na^+-modified catalyst surface. The H_2/CO-TPSR results showed that cobalt sites would adsorb CO dissociatively, propagate hydrocarbon chain, and hydrogenate the intermediate products, while copper atoms are known to adsorb CO associatively [20,43,49,52]. Because of the coexistence of both cobalt and copper in the structure of the perovskite precursor promoted with Na^+, these two metal sites are in close vicinity, so that a fast transfer of an alkyl group into an alkyl-CO species is facilitated to produce either straight alcohols or higher hydrocarbons [2,23,33,52]. Therefore, both hydrocarbons and alcohol products are consistent with an ASF distribution (Table 2) [42]. The propagation constant of alcohols is estimated from ASF plots for ethanol to heptanol (excluding methanol), while that of hydrocarbons is built from methane to undecane. As seen from Table 2, the ground Co–Cu-based perovskites show a close value of carbon chain growth probability for both alcohols and hydrocarbons, indicating the carbon skeleton of these products formed over the same active sites over the reduced ground perovskites. In this case, a higher partial pressure of CO will be favorable for the formation of higher alcohols. This explained the absence of alcohol signals during TPSR tests under atmospheric pressure. The alpha value of hydrocarbons is, however, significantly different from the one of alcohols obtained over the reduced Co-based perovskite precursors (GM0). This strongly supports the assumption that the role of copper is to facilitate the insertion of CO molecule into alkyl groups in order to produce higher alcohols instead of the corresponding hydrocarbons [20,33,52,53].

4. Conclusion

The reducibility of the ground perovskites is somewhat different from that of the citrate-derived samples. $LaCoO_3$ prepared by mechano-synthesis shows a number of distinct Co^{3+} ions in perovskite lattice, which are more reducible. Under controlled conditions, the reduction of cobalt ions occurs in two consecutive steps: Co^{3+}/Co^{2+} and Co^{2+}/Co^0,

while the intra-lattice copper ions are directly reduced from Cu^{2+} to Cu^0. The formation of copper atoms promotes the reducibility of cobalt ions, which is reduced at a relatively lower temperature. Therefore, a high dispersion of cobalt–-copper metals is obtained after reduction pretreatment. The reduction temperature of the nanocrystalline perovskites is dependent on the calcination temperature, catalyst morphology, particle size, and the amount of remnant sodium ions. The first reduction step is very sensitive to any change in the catalyst surface. The reduced form of lanthanum cobaltite perovskite could completely convert into the original structure after re-oxidation, whereas those of Co–Cu-based samples yield a mixture of oxides under the same experimental conditions.

The reduced catalyst surface comprising cobalt and copper atoms is rather selective for the hydrogenation of CO. The cobalt atom plays the role of an active site for CO dissociation, carbon chain growth, and hydrogenation but the presence of a neighboring copper has significantly affected the reactivity of cobalt. The addition of copper into perovskite framework and the presence of remnant sodium lead to changes in product distribution of the CO hydrogenation reaction and decrease the reaction temperature. The presence of copper sites in close proximity to cobalt atoms strongly affects the reactivity of carbonaceous species on the catalyst surface and facilitates the formation of alcohols, while that of sodium additive inhibits the methanation and promotes the formation of longer carbon-chain products. Under the synthesis conditions, the reduced nanocrystalline perovskites produced a mixture of higher alcohols, hydrocarbons, carbon dioxide, and water, while the citrate-derived samples produce mainly methane and light hydrocarbons. An increased amount of the ground intra-perovskite lattice copper leads to a substantial decrease in the rate of methanation and an increase in both selectivity and productivity of higher alcohols. The selectivity and the productivity of products are strongly dependent on the catalyst preparation, pretreatment conditions, alkali additive, and crystal domain sizes. The present and still preliminary reaction results of CO hydrogenation indicate that the reduction of nanocrystalline Co–Cu-based perovskites yields promising catalysts for the synthesis of hydrocarbons and higher alcohols from syngas.

Acknowledgments

Financial support of NSERC through its industrial chair program is gratefully acknowledged. The authors also thank Nanox Inc., Québec, Canada, for preparing the nanocrystalline ground perovskites and for financial support.

References

[1] F.S. Galasso, Structure, Properties and Preparation of Perovskite-Type Compounds, Pergamon Press, Oxford, 1969.
[2] M.A. Pena, J.L.G. Fierro, Chem. Rev. 101 (2001) 1981–2017.
[3] A. Cimino, F.S. Stone, Adv. Catal. 47 (2002) 141–306.
[4] T. Nitadori, M. Misono, J. Catal. 93 (1985) 459–466.
[5] T. Nitadori, S. Kurihara, M. Misono, J. Catal. 98 (1986) 221–228.
[6] S.M.D. Lima, J.M. Assaf, Catal. Lett. 108 (2006) 63–70.
[7] L.B. Sis, G.P. Wirtz, S.C. Sorenson, J. Appl. Phys. 44 (1973) 5553–5559.
[8] M. Crespin, W.K. Hall, J. Catal. 69 (1981) 359–370.
[9] J.O. Petunchi, M.A. Ulla, J.A. Marcos, E.A. Lombardo, J. Catal. 70 (1981) 356–363.
[10] R. Lago, G. Bini, M.A. Pena, J.L.G. Fierro, J. Catal. 167 (1997) 198–209.
[11] V.R. Choudhary, K.C. Mondal, A.S. Mamman, U.A. Joshi, Catal. Lett. 100 (2005) 271–276.
[12] L. Bedel, A.C. Roger, C. Estournes, A. Kiennemann, Catal. Today 85 (2003) 207–218.
[13] J.A.B. Bourzutschky, N. Homes, A.T. Bell, J. Catal. 124 (1990) 52–72.
[14] N. Tien-Thao, H. Alamdari, M.H. Zahedi-Niaki, S. Kaliaguine, Appl. Catal. A 311 (2006) 204–212.
[15] J.O. Petunchi, J.L. Nicastro, E.A. Lombardo, J. Chem. Soc., Chem. Commun. (1980) 467–468.
[16] N. Mouaddib, V. Perrichon, G.A. Martin, Appl. Catal. A 118 (1994) 63–72.
[17] G. Forasari, A. D'Huysser, L. Mintchev, T. Trifiro, A. Vaccaria, J. Catal. 135 (1992) 386–399.
[18] J.E. Baker, R. Burch, S.E. Golunski, Appl. Catal. 53 (1989) 279–297.
[19] J.E. Baker, R. Burch, S.J. Hibble, P.K. Loader, Appl. Catal. 65 (1990) 281–292.
[20] P. Courty, D. Durand, E. Freund, A. Sugier, J. Mol. Catal. 17 (1982) 241–254.
[21] J.P. Hindermann, G.J. Hutchings, A. Kiennemann, Catal. Rev. Sci. Eng. 35 (1993) 1–127.
[22] R.M. Bailliard-Letournel, A.J.G. Cobo, C. Mirodatos, M. Primet, J.A. Dalmon, Catal. Lett. 2 (1989) 149–156.
[23] M. Blanchard, H. Derule, P. Canesson, Catal. Lett. 2 (1989) 319–322.
[24] G.R. Sheffer, R.A. Jacobson, T.S. King, J. Catal. 116 (1989) 95–107.
[25] S. Kaliaguine, A.V. Neste, V. Szabo, J.E. Gallot, M. Bassir, R. Muzychuk, Appl. Catal. A 209 (2001) 345–358.
[26] H.P. Klug, L.E. Alexander, Procedures for Polycrystalline and Amorphous Materials, Wiley, New York/London, 1962.
[27] S. Royer, H. Alamdari, D. Duprez, S. Kaliaguine, Appl. Catal. B 58 (2005) 273–288.
[28] J.L.G. Fierro, M.A. Pena, L.G. Tejuca, J. Mater. Sci. 23 (1988) 1018–1023.
[29] B. Echchahed, H. Alamdari, S. Kaliaguine, Int. J. Chem. React. Eng. 4 (2006) A29.
[30] E.A. Lombardo, K. Tanaka, I. Toyoshima, J. Catal. 80 (1983) 340–349.
[31] P. Porta, S.D. Rossi, M. Faticanti, G. Minelli, I. Pettiti, L. Lisi, M. Turco, J. Solid State Chem. 146 (1999) 291–304.
[32] L. Lisi, G. Bagnasco, P. Ciambelli, S.D. Rossi, P. Porta, G. Russo, M. Turco, J. Solid State Chem. 146 (1999) 176–183.
[33] J.A. Dalmon, P. Chaumette, C. Mirodatos, Catal. Today 15 (1992) 101–127.
[34] L. Huang, M. Bassir, S. Kaliaguine, Appl. Surf. Sci. 243 (2005) 360–375.
[35] S. Irusta, M.P. Pina, M. Menendez, J. Santamaria, J. Catal. 179 (1998) 400–412.
[36] J. Szekely, J.W. Evans, H.Y. Sohn, Gas–Solid Reactions, Academic Press, New York, 1976.
[37] N. Tien-Thao, M.H. Zahedi-Niaki, H. Alamdari, S. Kaliaguine, J. Catal. 245 (2007) 348–357.
[38] M.J.L. Gines, E. Iglesia, J. Catal. 176 (1998) 155–172.
[39] J.A. Marcos, R.H. Buitrago, E.A. Lombardo, J. Catal. 105 (1987) 95–106.
[40] J.M. Campos-Martin, J.L.G. Fierro, A. Guerrero-Ruiz, R.G. Herman, K. Klier, J. Catal. 163 (1996) 418–428.

[41] W.H. Lee, C.H. Bartholomew, J. Catal. 120 (1989) 256–271.
[42] T. Herranz, S. Rojas, F.J. Perez-Alonso, M. Ojeda, P. Terreros, J.L.G. Fierro, J. Catal. 243 (2006) 199–211.
[43] F.M.T. Mendes, C.A.C. Perez, F.B. Noronha, M. Schmal, Catal. Today 101 (2005) 45–50.
[44] S.Z. Ozdogan, P.D. Gochis, J.L. Falconer, J. Catal. 83 (1983) 257–266.
[45] M. Ojeda, M.L. Granados, S. Rojas, P. Terroros, F.J. Garcia-Garcia, J.L.G. Fierro, Appl. Catal. A 261 (2004) 47–55.
[46] B.H. Sakakini, J. Mol. Catal. A 127 (1997) 203–209.
[47] R.B. Anderson, The Fischer–Tropsch Synthesis, Academic Press, New York, 1984.
[48] W.H. Lee, C.H. Bartholomew, J. Catal. 120 (1989) 256–271.
[49] V. Ponec, Catal. Today 12 (1992) 227–254.
[50] W.A.A.V. Barneveld, V. Ponec, J. Catal. 51 (1978) 426–430.
[51] W.A.A.V. Barneveld, V. Ponec, J. Catal. 89 (1984) 542–544.
[52] X. Xiaoding, E.B.M. Doesburg, J.J.F. Scholten, Catal. Today 2 (1987) 125–170.
[53] P. Chaumette, P. Courty, A. Kiennemann, B. Ernst, Top. Catal. 2 (1995) 117–126.
[54] P. Forzatti, E. Tronconi, I. Pasquon, Catal. Rev. Sci. Eng. 33 (1991) 109–168.
[55] S. Li, A. Li, S. Krishnamoorthy, E. Iglesia, Catal. Lett. 77 (2001) 197–205.
[56] S.B. Lee, M. Weiss, G. Ertl, Surf. Sci. 108 (1981) 357–367.